Bulletin of the Seismological Society of America, Vol. 85, No. 3, pp. 834–844, June 1995

The Log (rms Lg)-m_b Scaling Law Slope

by Xiao-Bi Xie and Thorne Lay

Abstract The Lg phase has been demonstrated to have unusual stability and precision of relative scaling with the global m_b or yield of nuclear explosions on a path by path basis. However, Lg scaling slopes with magnitude for different propagation paths are often quite different, an unexplained effect which complicates nuclear monitoring procedures. In this study, both data analysis and numerical simulations are used to explore the factors influencing Lg scaling. Digital seismic data from broadband stations in Eurasia for explosions at the former Soviet Union nuclear test site in Balapan are analyzed. The data suggest that yield scaling of the source spectrum, combined with frequency selection properties of propagation on each path are responsible for the observed variations in scaling slope. Loss of high-frequency energy by attenuation causes high scaling slopes along some paths. Variations in site effects and instrument responses may also contribute to the scatter of Lg scaling slopes. Numerical simulations, used to calculate synthetic scaling laws, support these inferences.

Introduction

The Lg phase is a complicated seismic signal comprised of many surface-wave higher modes having group velocities near 3.5 km/sec with the energy being strongly scattered by crustal heterogeneities (e.g., Knopoff *et al.*, 1973; Bouchon, 1982; Kennett, 1985; Nuttli, 1986, 1988; Xie and Lay, 1994). The intrinsic complexity of Lg provides very effective averaging of both the source radiation and the effects of crustal structure along a particular path. These characteristics make statistical measures of Lg, such as the rms amplitude over a specified group velocity window, very stable and accurate relative source-strength estimates for use in nuclear test discrimination and yield estimation, as well as for determining earthquake magnitudes. However, one of the interesting aspects of Lg is that while rms observations for a given path show small variance in yield scaling, the slope of rms Lg measurements as a function of magnitude or yield may differ for different paths (Hansen *et al.*, 1990; Israelsson, 1992; Gupta *et al.*, 1992). Understanding the cause of variations in Lg-yield scaling slope will improve our ability to exploit Lg for low-threshold treaty monitoring.

The empirical relationship between Lg amplitude and yield at a fixed epicentral distance and for a given station is usually represented as (e.g., Richards, 1989) $A_{Lg} = CY^{\alpha}$, where A_{Lg} is some robust but bandlimited measure of Lg amplitude, Y is yield, and C and α are parameters. On a logarithmic scale, we obtain the scaling relation $\log (A_{Lg}) = \log (C) + \alpha \log (Y)$, where α is the slope of the scaling law of primary interest for this study. Equivalently, $\log (Y)$ can be replaced with m_b and a slightly different slope. Many factors, including source excitation parameters and propagation effects, influence the Lg amplitude through their effects on α and C. Most of the source parameters depend linearly or nonlinearly on the yield, so aside from coupling effects they primarily influence α. But, given that scaling slope changes can be observed for Lg phases on different paths for the same group of events at the same test site, the source effect cannot be the only factor affecting the scaling slope. On the other hand, propagation effects should contribute primarily to the parameter C. Effects such as attenuation, blockage, and degree of scattering can make the logarithmic scaling relation shift up or down on a given path, but these linear effects should not directly affect the slope of the scaling relation since they are common to all events on that path. A viable explanation is that the parameter α is frequency dependent, i.e., the scaling slope is different at different frequencies. The factor C, which serves as a frequency weighing function, determines which part of the frequency content contributes to the observed bandlimited amplitude on a given path. The combination of both factors, the frequency-dependent source scaling and bandlimiting propagation effect, can then generate the observed scaling slope changes between paths.

Frequency-dependent scaling relations of explosion sources and their effects on body waves, surface waves, and regional waves have long been recognized (e.g., Mueller and Murphy, 1971; von Seggern and Blandford, 1972). Narrowband amplitude measures can exhibit frequency-dependent yield scaling due to yield dependence of the source spectral corner frequency. In addition, a given measure, such as m_b, can scale differently at different stations if attenuation variations enhance the apparent corner frequency shift in the relevant passband. Lay *et al.* (1984) investigated broadband

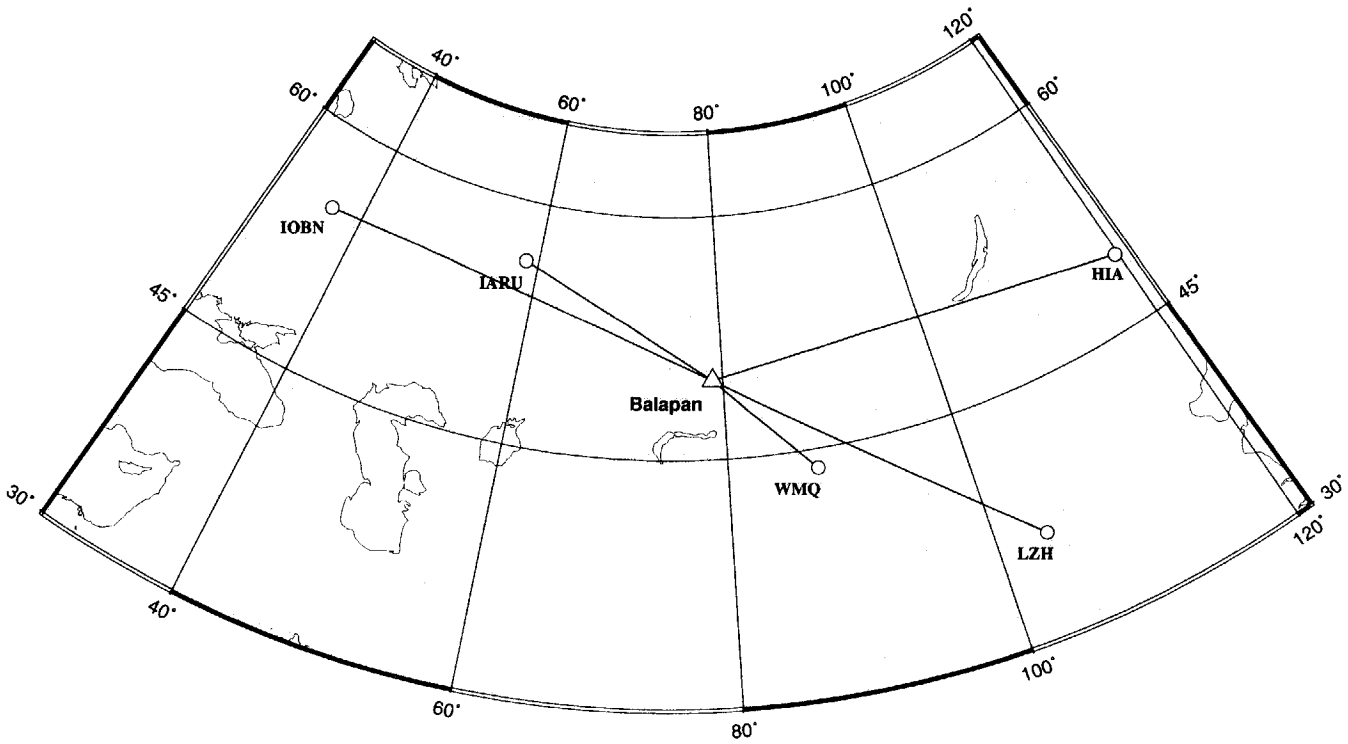

Figure 1. Map showing the locations of the Balapan test site (triangle) and the digital stations (open circles) from IRIS and CDSN networks used in this study. The epicentral distances for the stations range from 950 to 2900 km (see Table 1).

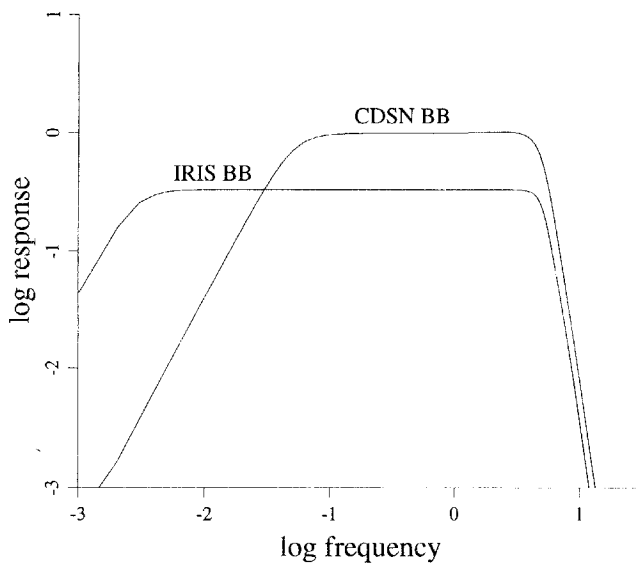

Figure 2. Representative frequency response curves for CDSN and IRIS digital stations. Ground-velocity responses are plotted to display the bandwidth of these broadband instruments.

seismic data for the three underground nuclear explosions at the Amchitka test site to obtain empirical yield-scaling behavior in the period range 0.2 to 20 sec. The results clearly indicate that short-period yield scaling obtained from m_b and P-wave amplitude observations in the period range 0.5 to 2.0 sec is quite different from long-period surface wave (M_s) yield scaling, even after correcting for propagation effects in each passband. This was interpreted as evidence for yield dependence of overshoot of the source-time functions. Ringdal and Fyen (1988) analyzed data from Semipalatinsk explosions recorded at the NORSAR and GRF arrays, and suggested that frequency scaling of the Lg source spectrum together with differences in instrument responses may account for an observed difference in Lg scaling slope between these arrays. Israelsson (1992) investigated a set of digitized historical Lg-wave recordings from six internal Soviet Union stations for explosions at Semipalatinsk and Novaya Zemlya. He suggested that frequency scaling of the Lg source spectrum, in combination with varying intrinsic attenuation and site responses, appears to give rise to variations in station Lg scaling. We will elaborate on this idea.

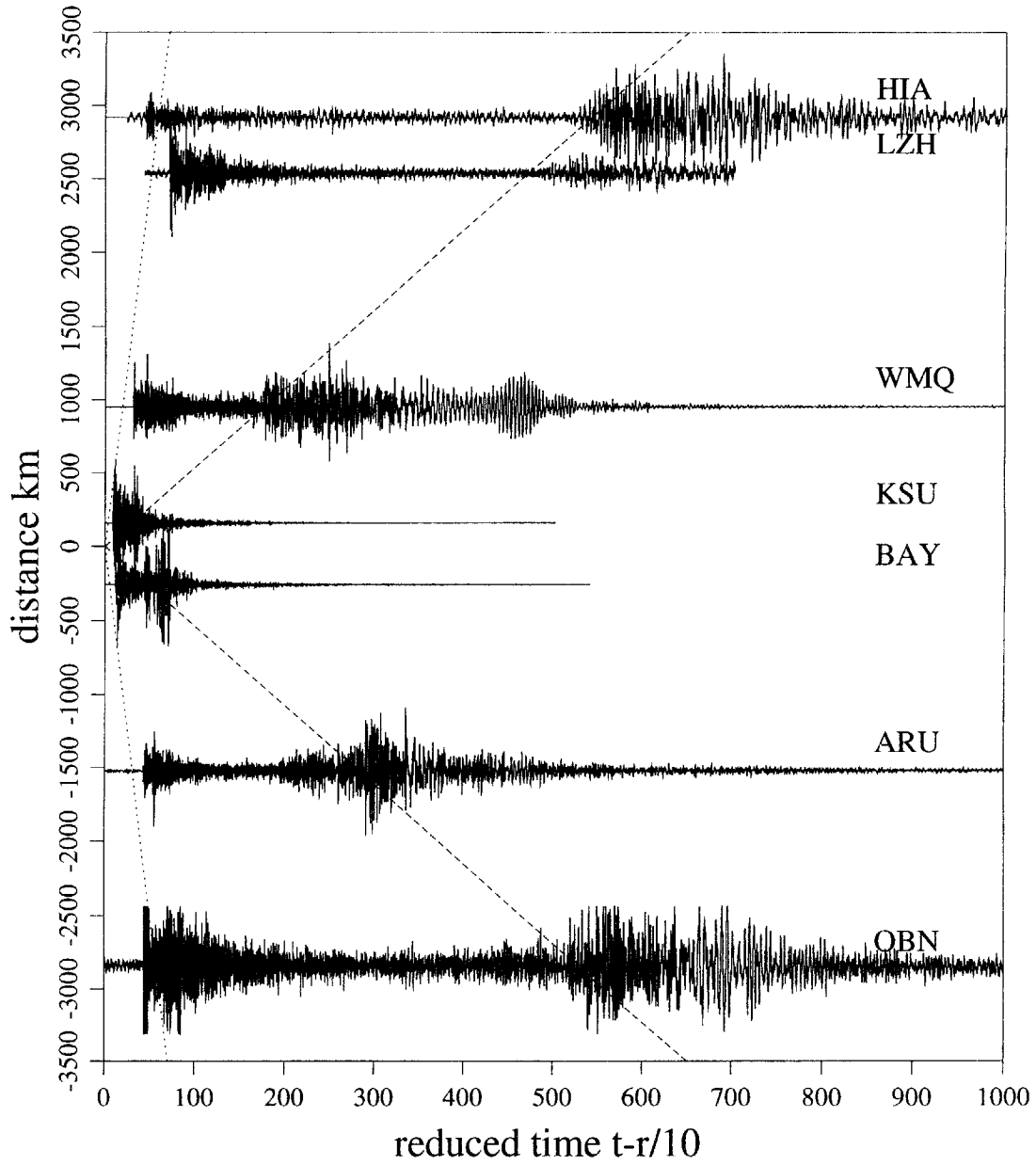

Figure 3. Typical seismograms from Balapan explosions recorded at Eurasian stations. The negative distances indicate stations to the west of the source and positive distances indicate stations to the east of the source. The dashed lines denote a group velocity of 3.5 km/sec, appropriate for the *Lg* phase, and the dotted lines denote a reference velocity of 8.33 km/sec.

Table 1
Locations of Seismic Stations

Station	Latitude	Longitude	Elevation (m)	Approximate Epicentral Distance from Balapan Test Site (km)
WMQ	43.82 N	87.70 E	970	952
HIA	49.27 N	119.74 E	610	2918
LZH	36.09 N	103.84 E	1560	2539
IARU	56.40 N	58.60 E	250	1526
IOBN	55.10 N	36.60 E	130	2875

In this study, digital broadband seismic records from IRIS and CDSN (Chinese Digital Seismic Network) stations for underground nuclear tests in the Balapan test site of the former Soviet Union are used to investigate *Lg* scaling slope variations. We first investigate several observations characterizing the frequency-dependent scaling relations. These indicate that scaling of the source spectrum combined with the frequency selection properties of the propagation effect can generate the observed scaling slope changes. Then, synthetic

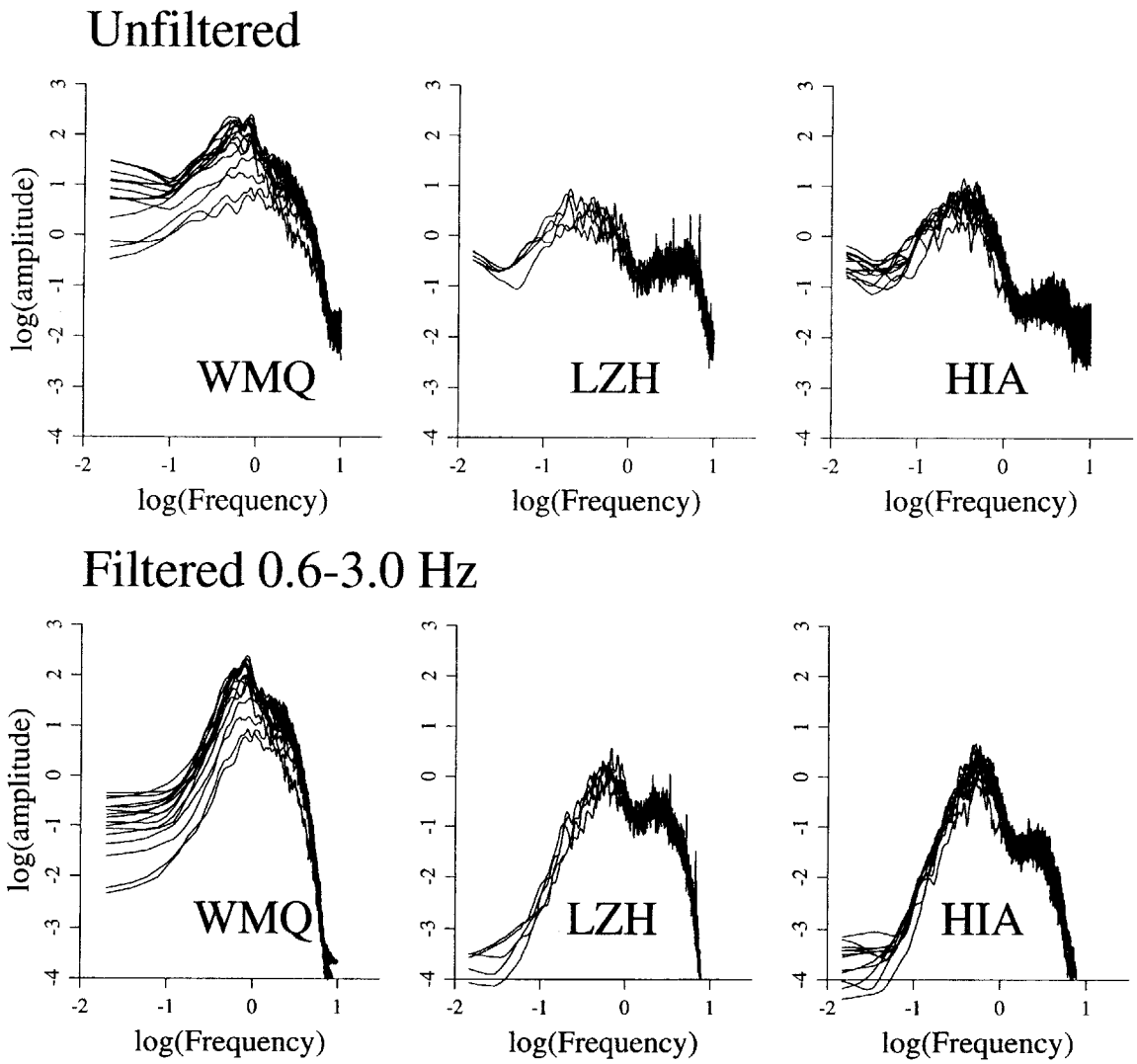

Figure 4. Velocity spectra from three CDSN stations. The upper row shows unfiltered spectra and the lower row shows spectra filtered between 0.6 and 3.0 Hz. Note that even after bandpass filtering, which is usually used for rms *Lg* measurement, frequency-dependent scaling behavior still exists.

scaling slopes calculated from numerical simulations are used to confirm these inferences.

Data

Figure 1 shows the locations of the Balapan test site and the digital stations used in this study. Three of the stations, WMQ, HIA, and LZH, belong to the CDSN and the other two stations, IARU and IOBN, are IRIS stations deployed in 1988. The epicentral distances for these stations range from 950 to 3000 km (Table 1), a typical distance range for *Lg* observations. All IRIS and CDSN stations are equipped with broadband instruments. Figure 2 shows the ground-velocity frequency responses for these stations. They have flat velocity response curves within a frequency band between 0.02 and 8 Hz. The *Lg* measurements are well within this frequency band, which ensures that this analysis will not be influenced by the instrument responses.

Figure 3 is a representative profile for *Lg* waves from underground explosions at Balapan recorded across Eurasia. The horizontal coordinate is reduced time with a reference velocity of 10 km/sec. The vertical coordinate is distance, with stations located to the west of Balapan indicated with negative distances while stations located to the east are plotted with positive distances. The dashed lines denote a 3.5-km/sec velocity, a typical group velocity for *Lg* phases. Dotted lines denote a reference velocity of 8.33 km/sec, which is roughly the *P*-wave velocity in the uppermost mantle in this region (Priestley, 1988). In addition to the IRIS and CDSN stations, records from two near-in stations KSU and BAY, are also shown here. These two stations were temporarily deployed during the Joint Verification Experiment

Table 2
Event List*

Date (m/d/yr)	m_b	WMQ	HIA	LZH	IARU	IOBN
06/20/1987	6.03	B	B			
08/02/1987	5.83	B	B			
11/15/1987	5.98	B	B			
12/13/1987	6.06	B	B			
12/27/1987	6.00	B	B			
04/03/1988	5.99	B	B			
09/14/1988	6.03	B	B		B	B
11/12/1988	5.24	B			B	
12/17/1988	5.83	B	B	B	B	
01/22/1989	6.01	B	B	B		
02/12/1989	5.86	B	B	B	B	
07/08/1989	5.55	B	B	B		
09/02/1989	4.94	B				B
10/19/1989	5.86	B	B	B	B	B

*B: available broadband digital data.

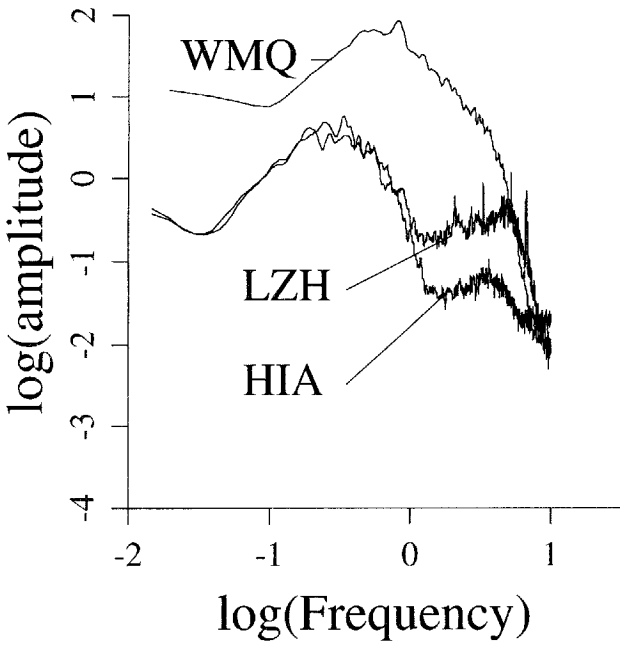

Figure 5. Average *Lg* velocity spectra for stations WMQ, LZH, and HIA. The spectra are averaged from three events (17 December 1988, 12 February 1989, and 19 October 1989) with similar m_b. The nearest station, WMQ, has more high-frequency signal than the more distant stations.

(JVE) (Priestley and Walter, 1990). All the seismograms in Figure 3 are vertical components from the JVE explosion except for the record at LZH, which is for a similar size event on 22 January 1989. For the JVE, the global m_b is 6.03 and the estimated yield is 113 kt (Sykes and Ekström, 1989). The most prominent feature in the figure is the well-developed *Lg* phase along these continental paths. The *Lg* amplitudes are well above the coda of preceding waves, which is

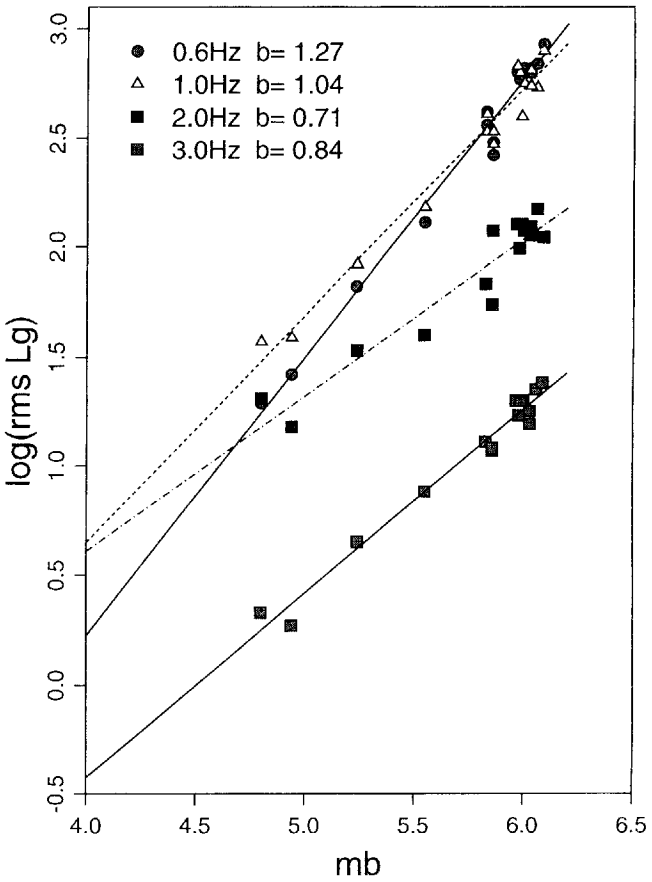

Figure 6. Scaling slopes of log rms *Lg* obtained from WMQ versus event m_b. Seismograms are filtered through different narrow passbands. Different symbols denote different center frequencies. The lower frequency signal has a larger scaling slope.

not always the case in Eurasia. The group velocity for the primary *Lg* waves is close to 3.5 km/sec in both propagation directions. For this reason, we choose a 3.2- to 3.7-km/sec velocity window for measuring *Lg* wave amplitudes throughout this study. A total of 14 events are analyzed here. Table 2 lists these events and the broadband data that are available at the regional stations. WMQ and HIA have the largest data sets, while LZH, IARU, and IOBN deployed digital systems more recently and provide fewer data.

Figure 4 presents the velocity spectra of *Lg* phases at the three CDSN stations for events of different magnitudes. Shown on the upper row are unfiltered spectra and on the lower row are filtered spectra. For the later case, before calculating the spectra, seismograms are filtered with a zero-phase Butterworth filter between 0.6 and 3.0 Hz, which is a commonly used passband for rms *Lg* measurements. A prominent feature in the data is the frequency-dependent scaling of these spectra. For smaller events the corner frequencies shift toward higher frequencies causing the spectra to span a larger amplitude interval at lower frequencies than that at higher frequencies. This will cause the scaling relation to be different between the low- and high-frequency pass-

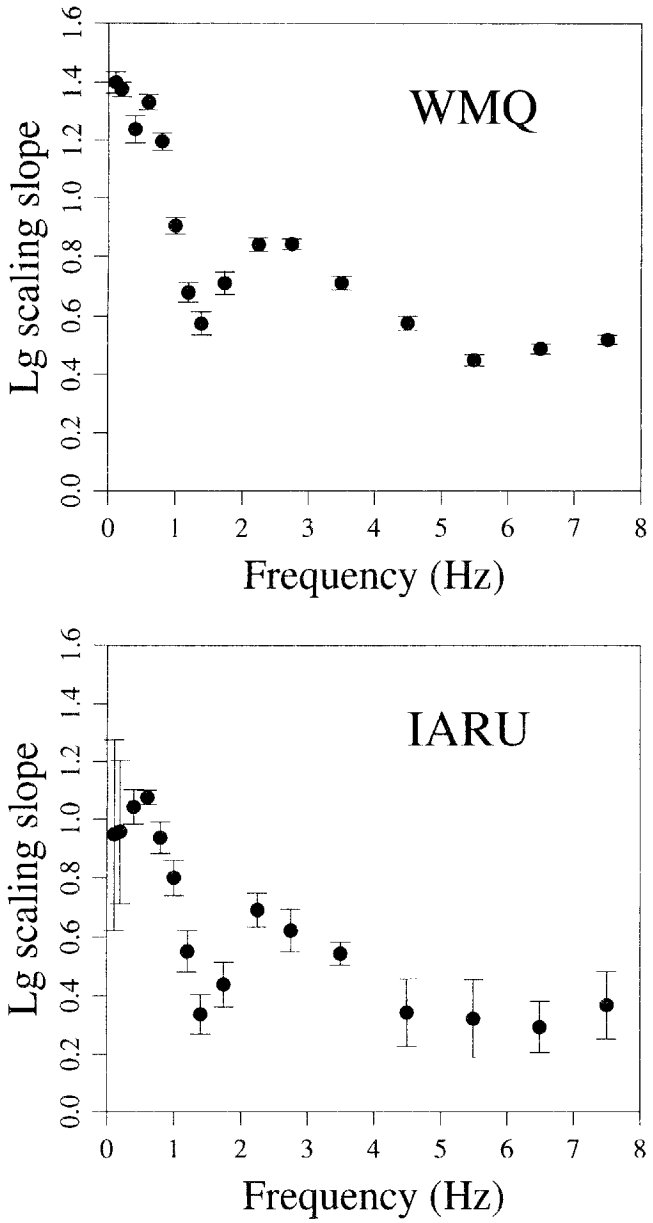

Figure 7. Log rms Lg-m_b scaling slopes as a function of frequency for stations WMQ and IARU. Seismograms are filtered by a series of narrow bandpass filters with different center frequencies. For frequencies lower than 1 Hz, the scaling slopes are larger than 1.0 and for higher frequencies the slopes decrease.

bands. This phenomenon is especially clear for station WMQ, for which the data cover the largest magnitude interval. The lower part of the figure shows that bandpass filtering reduces, but does not eliminate this effect. It is analogous to the source spectral differences that cause differences in scaling slope for M_s and m_b measurements.

We assume that the source spectrum of the Lg phases is basically azimuthally independent for an explosion source. Thus, frequency-dependent source scaling alone cannot account for differences in the spectra or in yield scaling, and we must consider propagation effects. The Lg propagation effects involve both elastic and anelastic structures of the crustal wave guide. Our limited knowledge of the crustal structure precludes us from reliably correcting for all propagation effects in our passband. Both intrinsic attenuation and scattering tend to remove more high-frequency energy than low-frequency energy. As the Lg phase propagates, the relative amplitude between the low- and high-frequency spectra is progressively modified. This can be clearly shown by comparing the spectra obtained from stations at different epicentral distances. The epicentral distances for WMQ, LZH, and HIA are 952, 2539, and 2918 km, respectively. In Figure 5, spectra from these stations are compared. Average spectra are calculated from three events (17 December 1988; 12 February 1989; and 19 October 1989), which have similar magnitudes and were recorded by all three stations. Figure 5 clearly shows that the high-frequency content is strongly attenuated at stations LZH and HIA compared to WMQ. As mentioned above, although statistical measurements of Lg are usually taken within a limited passband, typical filtering cannot completely eliminate the frequency-dependent scaling. Consequently, differences in attenuation of high-frequency signal will affect the Lg measurement.

Scaling Slope

It is expected that the overall explosion source scales differently at different frequencies and this appears to be true for the effective Lg source as well. Propagation effects can then enhance the behavior, causing variable scaling on different paths. The low- and high-frequency signals attenuate differently depending on the propagation distances and/or anelastic properties for a specific path. Signals that undergo high attenuation will be dominated by the scaling at low frequencies, which tends to have a higher scaling slope. This can explain an observation by Hansen *et al.* (1990). When comparing the rms Lg scaling slopes for several Shagan River explosions at IRIS, CDSN, and NORSAR stations, they found that the station HIA has the highest scaling slope. This is probably caused by its large epicentral distance and/or high attenuation on the path across Lake Baikal. We need to assess how strong this effect is and whether we can isolate it.

At a specific station, the scaling slope depends on the frequency band used for processing the data. Shown in Figure 6 are m_b—rms Lg amplitude scaling slopes in different passbands obtained for station WMQ. The seismograms are filtered by a series of zero-phase Butterworth filters with frequency bands 0.4 to 0.8, 0.7 to 1.3, 1.5 to 2.5 and 2.5 to 3.5 Hz, and then the time domain rms amplitudes of Lg are calculated within the 3.2- to 3.7-km/sec group-velocity window. In Figure 6, different symbols denote different center frequencies. For this station, the scaling slope obtained using the relatively broad 0.6- to 3.0-Hz frequency band is about 1, while the scaling slopes obtained from narrow bandpass filters with different center frequencies are quite different.

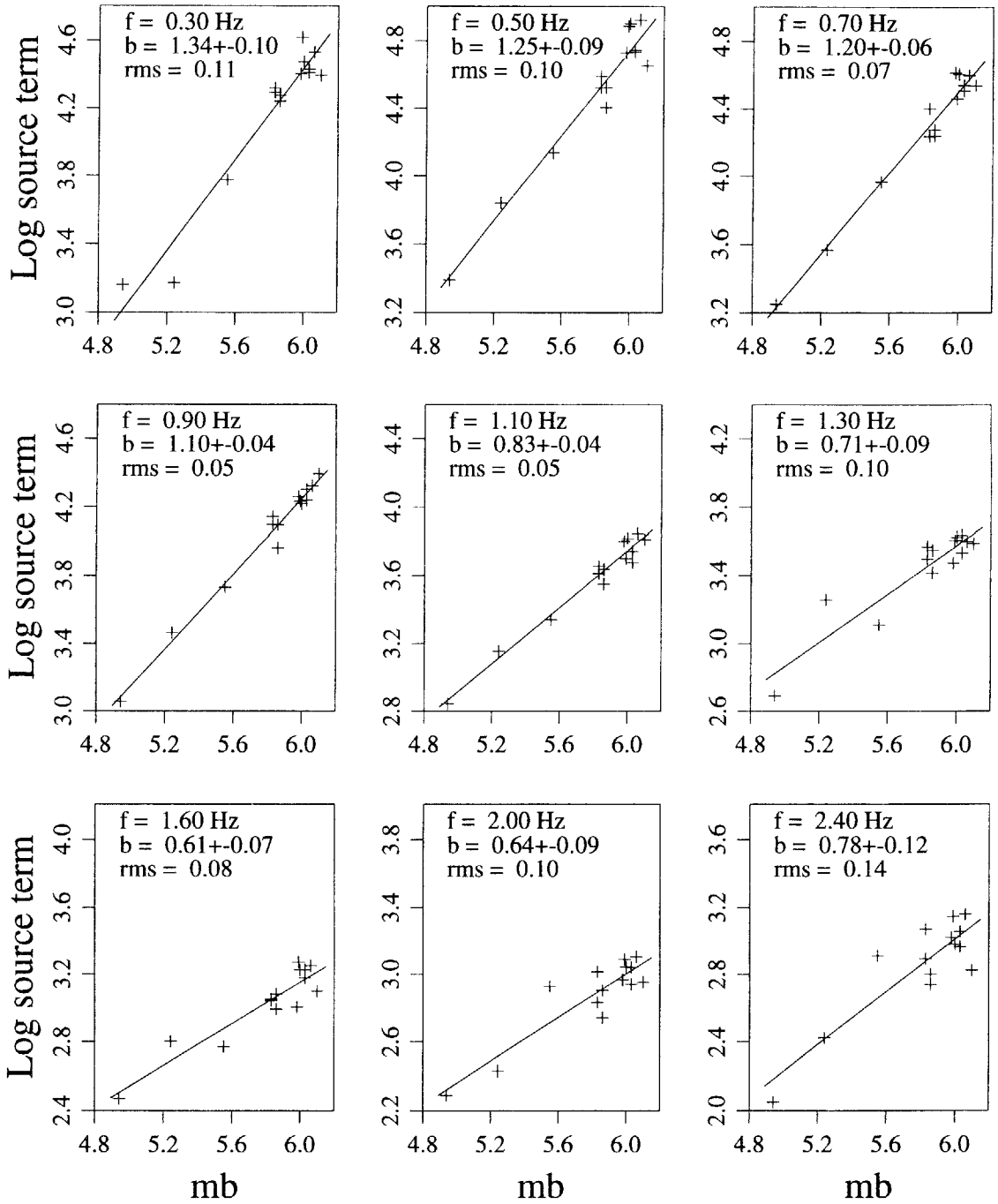

Figure 8. Source terms at different frequencies as a function of event m_b. The source terms are inverted from the data set listed in Table 2. At each frequency, the source terms have been fit with a straight line. The center frequency, scaling slope and the standard deviations for slope and data points are listed on each figure.

Lower frequency passbands have larger scaling slope. Figure 7 gives the scaling slopes as a function of frequency for stations WMQ and IARU. The error bars indicate the standard deviations of the slopes. For frequencies lower than 1 Hz, the scaling slopes are larger than 1.0 and for higher frequencies the slopes decrease. The two stations show generally the same trend except that the standard deviations are larger for IARU, a result of the smaller data set for this station and lack of small events.

The frequency dependence of *Lg* scaling slope may also be observed in *Lg* source terms. We calculated the source terms for 14 Balapan nuclear explosions using the digital broadband data. Following Israelsson (1992), for a given center frequency f, we assume that the logarithm of the rms

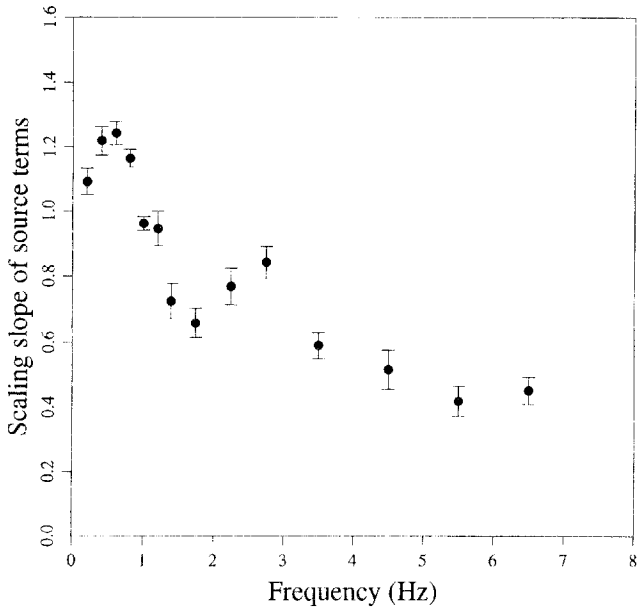

Figure 9. Scaling slope of the source terms in Figure 8 as a function of frequency.

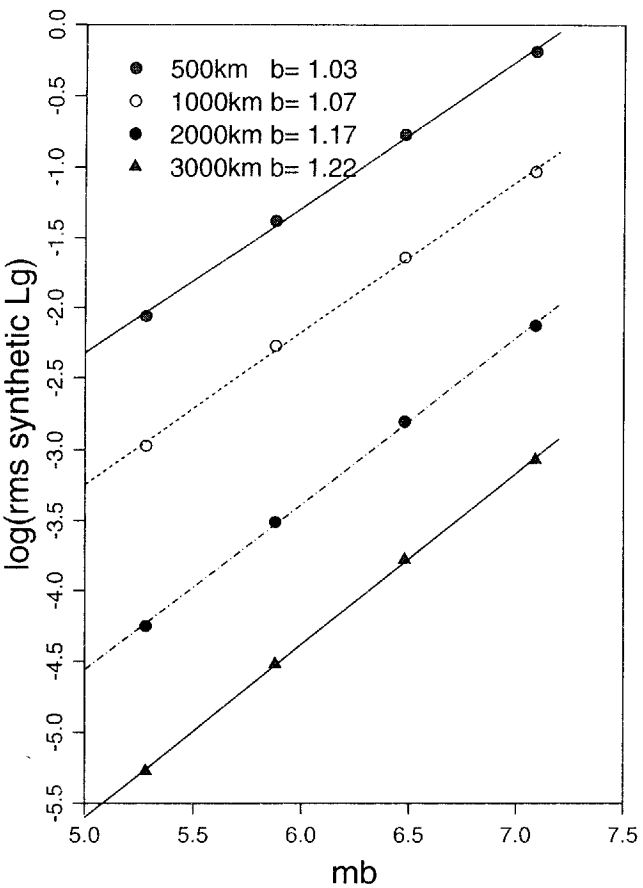

Figure 10. Synthetic log rms Lg-m_b scaling slopes obtained from epicentral distances of 500, 1000, 2000, and 3000 km.

amplitude, $A(f)$, can be separated into a source term $S(f)$, a station correction $T(f)$, and a path term. Furthermore, the path term can be resolved into a geometrical spreading factor G, and a nongeometric attenuation term that is characterized by a frequency-dependent attenuation coefficient $\gamma(f)$. The system that links all the events and observations can be written as

$$S_i(f) + T_j(f) = A_{ij}(f) - G(\Delta_{ij}) + \gamma(f)\Delta_{ij} \log(e) + \varepsilon_{ij}, \quad (1)$$

where $A_{ij}(f)$ is the observed logarithmic rms amplitude for the ith event at the jth station calculated after passing the seismogram through a filter with central frequency f, Δ_{ij} is the epicentral distance from the ith event to the jth station, and ε is an error term. For geometric spreading, Nuttli (1973) suggested that the standard formula for an Airy phase derived by Ewing *et al.* (1957) can be adopted to describe the Lg phase. The attenuation coefficient can be expressed as $\gamma(f) = \pi f/QU$, where U is the group velocity and Q is a frequency dependent, apparent quality factor that includes the effects of intrinsic attenuation and scattering of the crustal wave guide. Israelsson (1992) obtained a model with $Q = 731f^{0.42}$ for the eastern U.S.S.R. Xie (1993) designed a nonlinear method for simultaneous inversion of Lg source spectra and path Q. With this method, he obtained path-dependent Q values from the Balapan test site to some IRIS and CDSN stations. We tested both Q models and found they give quite similar results for the source term scaling slopes. For simplicity, here we use Israelsson's results for a path-independent $\gamma(f)$. The observed seismograms are corrected for the instrument responses and then passed through a series of zero-phase Butterworth filters. The bandwidths are 0.2 Hz for center frequencies 0.1 to 1.5 Hz, 0.5 Hz for center frequencies 1.75 to 2.75 Hz, and 1.0 Hz for center frequencies 3.5 to 6.5 Hz. A least-squares algorithm based on the singular value decomposition (Lawson and Hanson, 1974) is used to solve equation (1).

Shown in Figure 8 are source terms obtained from equation (1) for different frequencies versus m_b. For each frequency, the source terms have been fit with a straight line. The center frequency, scaling slope and its standard deviation, and the standard deviations of the data are listed on each small figure. At frequencies below 1.0 Hz, the scaling slopes are between 1.0 and 1.3, while above 1.0 Hz, the slopes fall to 0.6 to 0.7. This result strongly indicates that the Lg source terms from nuclear explosions do indeed scale differently for lower and higher frequency components for sources in the magnitude 5 to 6 range. The high quality of the broadband digital data enables us to obtain a reliable result with a relatively small data set. The result is similar to that obtained by Israelsson (1992), but our broadband data extend the frequency band to higher frequencies than his digitized analog data. Figure 9 gives the scaling slope of the source terms as a function of frequency. This figure shows

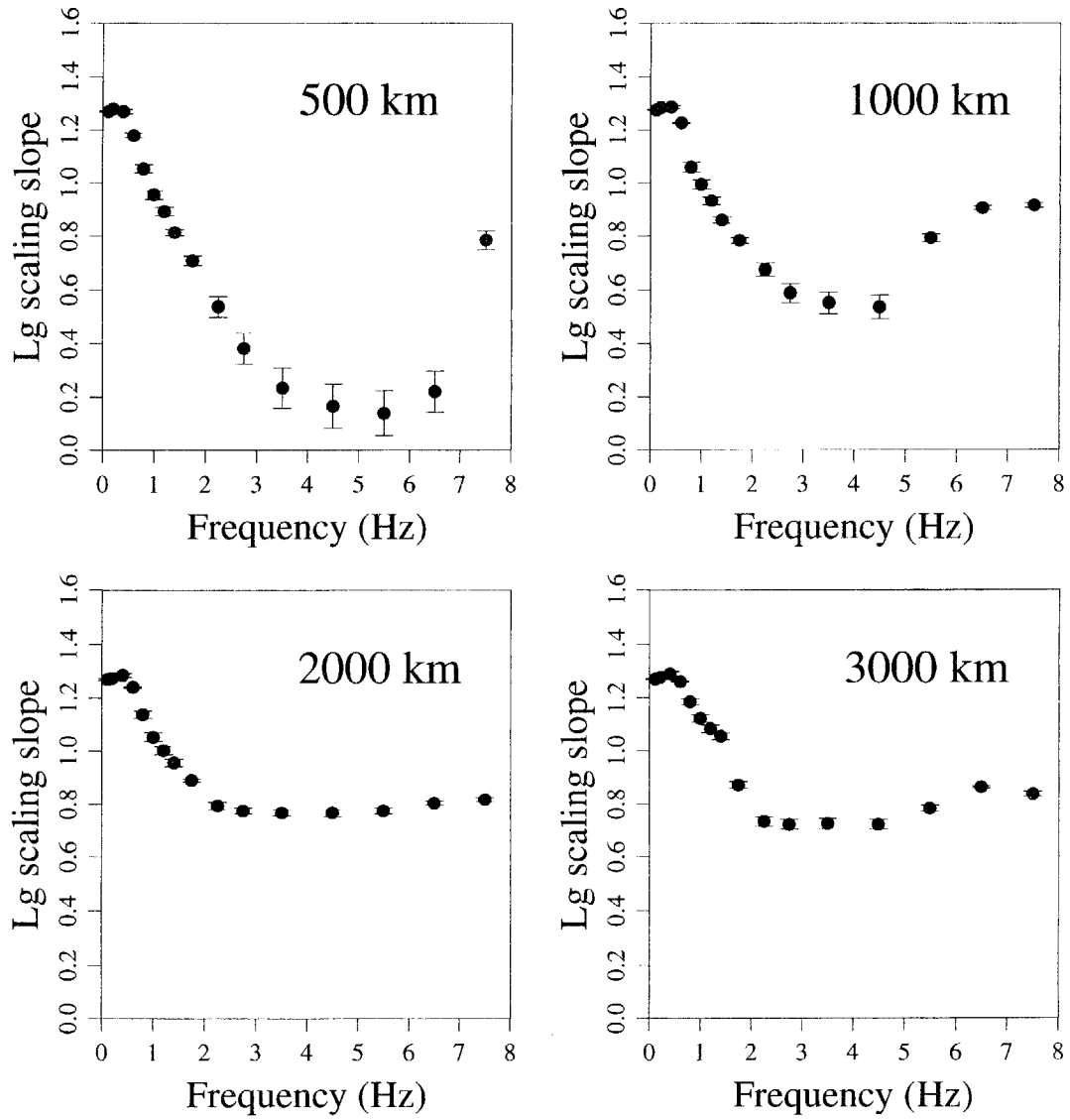

Figure 11. Synthetic log rms Lg-m_b scaling slopes versus frequency. The calculations show similar features to the real data (Fig. 7).

similar behavior to that in Figure 7. This suggests that the scaling slope directly obtained from narrow-band Lg data approximates the source scaling slope, despite the presence of propagation effects which mainly contribute to the intercept of the scaling law.

Numerical Simulations of Lg Scalling Law

A numerical simulation is conducted to establish how strongly attenuation can affect the Lg-wave scaling slope. We calculate synthetic seismograms with a mode summation method (Herrmann, 1979; Wang and Herrmann, 1980). A horizontally layered model similar to the crustal structure in East Kazakh (Priestley, 1988) is used in the calculations. To incorporate the intrinsic attenuation in the crustal wave guide, we set $Q_P = 600$ and $Q_S = 800$ in the crust and $Q_P = 2000$ and $Q_S = 1000$ in the upper mantle. These homogeneous model synthetics are not meant to produce waveforms in exact agreement with the data. The Mueller–Murphy source (Mueller and Murphy, 1971; Murphy, 1977) is adopted to generate the source-time function. The yields used in the calculations are 1, 10, 100, and 1000 kt. To facilitate comparison with the real data, the yield in the Muller–Murphy source needs to be transferred into m_b. Several empirical relations have been proposed to link the global body-wave magnitude m_b to the yield of Soviet explosions. Estimates of the slope between m_b and log yield range from 0.426 to 0.973 (Sykes and Ruggi, 1988; Israelsson, 1992). The Mueller–Murphy source was originally designed for NTS explosions instead of Soviet explosions. It gives a slope of 0.76 between the log amplitude and log yield at low frequency. To match the observation that, at low frequency, the

scaling slope between the log *Lg* amplitude and m_b is slightly larger than unity for Balapan events, we choose a slope of 0.6 between m_b and log yield to transfer the yield into m_b. Our intent here is just to have a realistic parameterization of the source spectrum scaling using a well-established explosion model adjusted to match the trend of the data, rather than to optimize parameters of the model.

Theoretical scaling slopes are calculated from the synthetic seismograms. A data analysis method similar to that applied to the real data is used to process the synthetics. Figure 10 gives the synthetic m_b scaling slopes for stations located at epicentral distances 500, 1000, 2000, and 3000 km. Scaling slopes are listed in the figure. For stations with larger epicentral distances, the scaling slopes are systematically higher. This is in agreement with trends in the real data. Figure 11 shows the scaling slope variations with frequency for the synthetics at each distance. Note that these trends are similar to Figure 7 for the real data. Instead of trying to match every detail of the real data, which depend on unknown fine structure of the crust, poorly constrained attenuation, and inaccurate source radiation models, we are content to demonstrate that the general features between the real and synthetic data are quite similar. Both have larger scaling slopes at lower frequencies and a sharp decrease above 1.0 Hz. The results show that for a laterally homogeneous structure and within the typical range for *Lg* observations, the scaling slope between log rms *Lg* amplitude and m_b can vary by up to 20%. The variation will be even larger given that the elastic and anelastic properties are actually different along different propagation paths. This explains the most important features systematically observed in the real data. Unfortunately, it appears that reliably correcting for path effects by anything other than a statistical approach is difficult, and nuclear monitoring procedures that use *Lg* data must accommodate the variations in yield scaling.

Discussion and Conclusion

In this study, both data analysis and numerical simulations are used to explore *Lg* scaling behavior. Digital seismic recordings at IRIS and CDSN stations for the former Soviet Union nuclear tests in Balapan are used for this purpose. Using narrow bandpass-filtered data, we find that at frequencies lower than 1 Hz, the *Lg*-m_b scaling slope is about 1.0 to 1.3, while for frequencies above 1 Hz, the slope decreases abruptly. This phenomenon suggests that scaling of the source spectrum, combined with the frequency selection properties of the propagation affects on each path, generate observed scaling slope variations. Numerical simulations are used to confirm this idea. *Lg* synthetic seismograms are calculated with the mode summation method for a horizontally layered crustal model and Mueller–Murphy source functions. Theoretical *Lg*-m_b scaling relations are obtained from the synthetic seismograms. The results show that a crustal model with moderate Q can cause the *Lg*-m_b scaling slope to change 20 to 30% over epicentral distances from 500 to 3000 km (typical observation distance for *Lg*). Loss of high-frequency signal by attenuation causes high scaling slopes along some paths. Site effects and instrument responses (if not properly corrected) may also contribute to the scatter of scaling slope, as will any bandlimiting effect which can interact with source-function scaling. These effects are analogous to those influencing body-wave scaling.

Acknowledgments

We thank Paul Richards for discussions on this topic, and Bob Herrmann for comments on the manuscript. This research was supported by the Advanced Research Projects Agency of the Department of Defense under Contract Number F29601-91-K-DB21, monitored by the Phillips Laboratory, and facilities were supported by the W. M. Keck Foundation. Contribution Number 234 of the Institute of Tectonics, University of California, Santa Cruz.

References

Bouchon, M. (1982). The complete synthesis of seismic crustal phases at regional distances, *J. Geophys. Res.* **78**, 1735–1741.

Ewing, W. M., W. S. Jardetsky, and F. Press (1957). *Elastic Waves in Layered Media*. McGraw Hill, New York.

Gupta, I. N., W. W. Chan, and R. A. Wagner (1992). A comparison of regional phases from underground nuclear explosions at east Kazakh and Nevada test sites, *Bull. Seism. Soc. Am.* **82**, 352–282.

Hansen, R. A., R. Ringdal, and P. G. Richards (1990). The stability of rms *Lg* measurements and their potential for accurate estimation of the yields of Soviet underground nuclear explosions, *Bull. Seism. Soc. Am.* **80**, 2106–2126.

Herrmann, R. B. (1979). *SH*-wave generation by dislocation source a numerical study, *Bull. Seism. Soc. Am.* **69**, 1–16.

Israelsson, H. (1992). RMS Lg as a yield estimator in Eurasia, Final Technical Report, PL-TR-92-2117(I), Phillips Laboratory, Hanscom Air Force Base, Massachusetts.

Kennett, B. L. N. (1985). On regional *S*, *Bull. Seism. Soc. Am.* **75**, 1077–1086.

Knopoff, L., F. Schwab, and E. Kausel (1973). Interpretation of Lg, *Geophys. J. R. Astr. Soc.* **33**, 389–404.

Lawson, C. L. and R. J. Hanson (1974). *Solving Least Squares Problems*, Prentice-Hall Inc., Englewood Cliffs, New Jersey.

Lay, T., D. V. Helmberger, and D. G. Harkrider (1984). Source models and yield-scaling relations for underground nuclear explosions at Amchitka island, *Bull. Seism. Soc. Am.* **74**, 843–862.

Mueller, R. A. and J. R. Murphy (1971). Seismic characteristics of underground nuclear detonations. Part I. Seismic spectrum scaling, *Bull. Seism. Soc. Am.* **61**, 1675–1692.

Murphy, J. R. (1977). Seismic source functions and magnitude determinations for underground nuclear detonations, *Bull. Seism. Soc. Am.* **67**, 135–158.

Nuttli, O. W. (1973). Seismic wave attenuation and magnitude relations for Eastern North America, *J. Geophys. Res.* **78**, 876–885.

Nuttli, O. W. (1986). Lg magnitudes of selected East Kazakhstan underground explosions, *Bull. Seism. Soc. Am.* **76**, 1241–1251.

Nuttli, O. W. (1988). Lg magnitudes and yield estimates for underground Novaya Zemlya nuclear explosions, *Bull. Seism. Soc. Am.* **78**, 873–884.

Priestley, K. F. (1988). Crustal structure in eastern Kazakh, U.S.S.R. from teleseismic receiver functions, *Geosphys. Res. Lett.* **15**, 613–616.

Priestley, K. F. and W. R. Walter (1990). Regional seismic recordings of the Soviet nuclear explosion of the joint verification experiment, *Geophys. Res. Lett.* **17**, 179–182.

Richards, P. G. (1989). Seismic monitoring of nuclear explosions, in *The*

Encyclopedia of Solid Earth Geophysics, D. E. James (Editor), Van Nostrand Reinhold Company, New York.

Ringdal, F. and J. Fyen (1988). Comparative analysis of NORSAR and Grafenberg Lg magnitudes of Shagan River explosions, in Semiann. Tech. Summ., 1 Apr-30 Sep 1988, NORSAR Sci. Report 1-88/89, Kjeller, Norway.

Sykes, L. R., and G. Ekström (1989). Comparison of seismic and hydrodynamic yield determinations for the Soviet joint verification experiment of 1988, *Proc. Natl. Acad. Sci. USA* **86**, 3456–3460.

Sykes, L. R. and S. Ruggi (1988). Soviet underground nuclear testing: inferences from seismic observations and historical perspective, in *Nuclear Weapons Data Book, Vol. IV, Soviet Nuclear Weapons*, Ballinger Publishing Company, Cambridge, Massachusetts.

von Seggern, D. and R. Blandford (1972). Source time functions and spectra for underground nuclear explosions, *Geophys. J.* **31**, 83–97.

Wang, C. Y. and R. G. Herrmann (1980). A numerical study of *P*-, *SV*-, and *SH*-wave generation in a plane layered medium, *Bull. Seism. Soc. Am.* **70**, 1015–1036.

Xie, J. (1993). Simultaneous inversion for source spectrum and path *Q* using *Lg* with application to three Semipalatinsk explosions, *Bull. Seism. Soc. Am.* **83**, 1547–1562.

Xie, X. B. and T. Lay (1994). The excitation of *Lg* waves by explosions: a finite-difference investigation, *Bull. Seism. Soc. Am.* **84**, 324–342.

Institute of Tectonics
University of California
Santa Cruz, California 95064

Manuscript received 20 March 1994.